Research Article

Lei Sheng*, Xue Zhengwei, Liu Yafeng, Li Yun, Jiang Dongsheng, and Wang Ping

Effect of annealing temperature on the structure and properties of FeCoCrNiMo high-entropy alloy

https://doi.org/10.1515/htmp-2022-0048
received March 25, 2022; accepted June 06, 2022

Abstract: FeCoCrNiMo high-entropy alloy was melted by vacuum arc melting. The alloys were vacuum annealed at 873, 1,073, and 1,273 K, respectively. X-ray diffractometer (XRD), scanning electron microscope (SEM), simultaneous thermal analyzer, microhardness tester, and universal testing machine were used to study the microstructure, the thermal stability, hardness and compression mechanics of as-cast and annealed FeCoCrNiMo alloys. The results show that the alloy is composed of face-centered cubic (FCC) phase and σ phase in both as-cast and annealed states, and the σ phase and μ phase can maintain structural stability at 873 K annealing temperature. The μ phase decomposes to form the σ phase after annealing at 1,073 K, and part of the σ phase dissolves in the FCC phase when annealed at 1,273 K. Both the as-cast and annealed alloys have a typical dendritic structure. The σ phase is enriched in dendrites, and the FCC phase exists between the dendrites. The microstructure of the alloys in the annealed state is more refined than that of the alloy in the as-cast state. In the 1,073 K annealed state, the FeCoCrNiMo alloy has the highest hardness, yield strength, and fracture strength. The fracture mechanism of the alloy is intergranular brittle fracture and cleavage fracture.

Keywords: high-entropy alloys, thermal stability, hardness, compressive properties, microstructure

*** Corresponding author: Lei Sheng,** School of Mechanical and Electrical Engineering, Anhui Jianzhu University, Hefei 230601, China; Key Laboratory of Intelligent Manufacturing of Construction Machinery, Hefei 230601, China, e-mail: leish1964@vip.126.com
Xue Zhengwei, Liu Yafeng, Li Yun, Jiang Dongsheng, Wang Ping: School of Mechanical and Electrical Engineering, Anhui Jianzhu University, Hefei 230601, China

1 Introduction

In recent years, high-entropy alloys (HEAs) have attracted more and more attention among material and engineering community because they show various exceptional properties, such as extraordinary strength and excellent mechanical properties at high temperature [1].

Usually, some Ni-base superalloys lead to the formation of Fe–Cr-rich TCP phase at 1,173 K, the generation of TCP phase will reduce the solution strengthening effect and decrease the mechanical properties of the alloy. Compared with traditional Ni-base superalloys [2], HEAs have higher stability at high temperature. Thus, they offer potential to replace high temperature materials such as Ni-based superalloys [3–5]. As advanced high-temperature structural materials, it is very necessary to study the thermal stability of high-entropy alloy in service [6,7].

Micro alloying of Mo was found to increase the strength of the FeCoCrNi-based HEA alloy, demonstrating the potential of utilizing the solute solution strengthening effect in HEAs. The study on the Mo-alloyed CoCrFeNi HEAs was reported by Shun et al. [8]. The CoCrFeNi alloy exhibits a single face-centered cubic (FCC) solid solution, whereas a (Cr,Mo)-rich σ phase is observed in the face-centered cubic matrix after the addition of Mo into the alloy. The hardness of face-centered cubic matrix and the compressive strength increase with the increase in the Mo concentration.

Nowadays, performance enhancement methods developed for traditional alloys have been successfully applied to HEAs, such as annealing, etc. A $CoCrFeNiMo_{0.3}$ alloy was 60% rolled and annealed under different conditions, and the σ and μ phases precipitated and strengthened the alloy. The alloy was obtained with a tensile strength of 1.2 GPa, and ductility of 19% [9].

In this work, the FeCoCrNiMo HEAs were prepared by vacuum arc melting. The microstructure evolution at different annealing temperatures was studied. The phase structure and mechanical properties of the alloy were determined. The thermal stability of FeCoCrNiMo alloys were discussed.

2 Experiment

2.1 Material preparation

Fe, Co, Cr, Ni, and Mo (purity >99.9 wt%) were smelted by vacuum arc melting on water-cooled plates in titanium-aspirated Ar gas. The arc-melted ingot was remelted at least five times to ensure the uniformity of composition. After natural cooling, a cylindrical sample with a diameter of 5 mm and a length of 10 mm is cut by wire cutting.

The as-cast and annealed alloys were ground and polished using a grinding machine (Buehler, USA). The microstructures of the samples were exposed after treatment by aqua regia for about 10 s. Then, the samples were subjected to vacuum annealing at 873, 1,073 K, and 1,273 K for 2 h. The surface microstructure of the samples was observed by SEM (Hitachi, Japan). The composition characteristic of as-cast and annealed alloys were analyzed by X-ray diffraction (XRD) (Panalytical, Netherlands). The hardness of the alloy was measured on the mirror surface of the specimen by microhardness tester (Wolpert Wilson, USA), which is set at a load of 0.2 kg with holding time of 15 s. Five measured points were spaced 5 mm apart on the specimen surface, and the average hardness value was calculated. Universal testing machine (Instron, USA) was used to test the compressive properties of the specimens at room temperature and the fracture microstructure was observed. Thermal analysis was performed using a simultaneous thermal analyzer (METTLER TOLEDO, Switzerland) at a heating rate of 20 K·min^{-1} under a flowing high-purity N2 atmosphere.

3 Results and discussion

3.1 XRD analysis

Figure 1 shows the XRD patterns of FeCoCrNiMo alloy in the as-cast state and at different annealing temperatures. The annealed FeCoCrNiMo alloy is still composed of FCC phase and σ phase, but the μ phase is not detected in the alloy at the annealing temperature of 1,073 K. The diffraction peak intensity of FCC phase in the as-cast state and at different annealing temperatures is the highest, indicating that the FCC phase is the main phase in the as-cast state and the annealing state at different temperatures.

The σ phase has a square structure (lattice parameters a = 9.2443 Å, c = 4.7921 Å, and c/a = 0.5183),

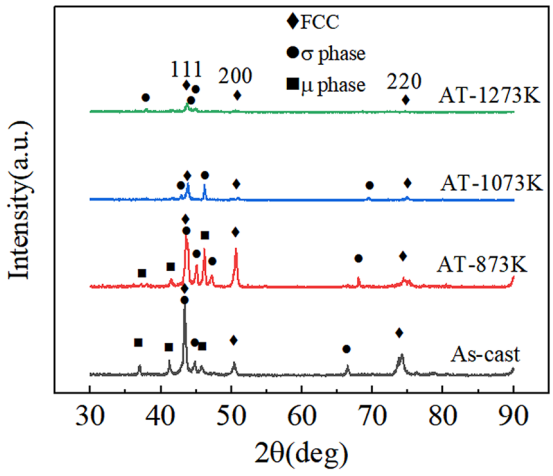

Figure 1: XRD patterns of as-cast and annealed FeCoCrNiMo alloys.

and the μ phase has a hexagonal structure (lattice parameters a = 3.5778 Å, c = 25.7538 Å, and c/a = 7.1982). The σ phase effectively increases the strength of the alloy, but reduces the plasticity of the alloy. Due to the increased hardness of the alloy, it is beneficial to improve the wear resistance of the alloy to some extent. The diffraction peak intensity of each phase decreases as the annealing temperature increases [10]. The annealing process enhances diffusion and substitution between elements, resulting in increased unit cell integrity and reduced lattice distortion. At 873 K, the intensity of the σ phase and μ phase diffraction peaks in the alloy is higher, indicating that the Mo-rich σ phase and μ phase can exist stably at 873 K. The μ phase is not detected in the XRD pattern at the annealing temperature of 1,073 K, indicating that the μ phase may be decomposed at 1,073 K.

3.2 Microstructure analysis

Figure 2 shows the microstructure of the FeCoCrNiMo alloy after annealing at different temperatures. The formation of a simple FCC solid solution is due to the fact that the atomic sizes of the four constituent elements, Fe, Co, Cr, and Ni, are approximately the same. There is no significant positive or negative enthalpy of mixing between the elements, as shown in Table 1.

The alloy has a typical dendritic structure after casting and heat treatment. The phases of the alloy can be divided into two regions. The main difference between these two regions is the enrichment of Co, Fe, and Ni elements between the dendrites, and the enrichment of Cr and Mo elements in the dendrites. The σ phase and μ phase are mainly distributed within the dendrites. XRD experiment

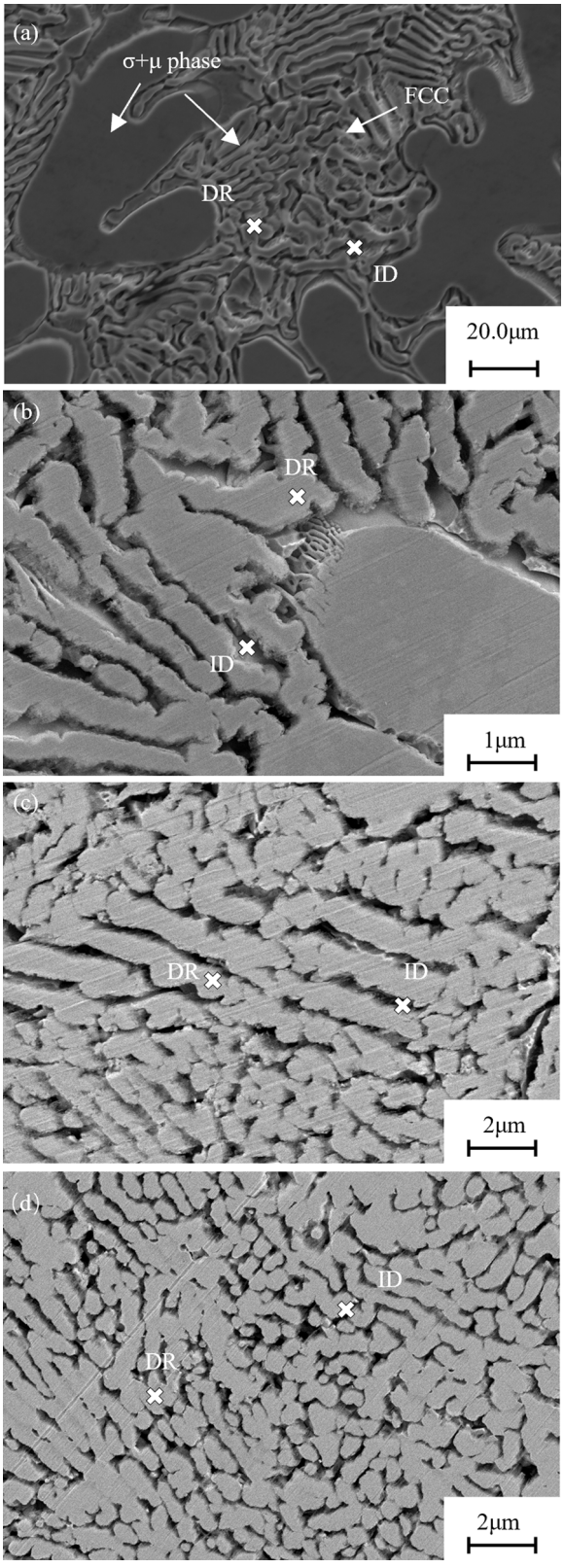

Figure 2: SEMimages of FeCoCrNiMo alloy at different annealing temperatures: (a) As-cast, (b) annealing treatment (AT)-873 K, (c) AT-1,073 K, and (d) AT-1,273 K.

Table 1: Binary mixing enthalpy (unit: kJ·mol^{-1}) and atomic sizes of different elements

Atomic radius (pm)	Co	Cr	Fe	Ni	Mo
Co (126 pm)	—	−4	−1	0	−5
Cr (127 pm)	−4	—	−1	−7	0
Fe (127 pm)	−1	−1	—	−2	−2
Ni (124 pm)	0	−7	−2	—	−7
Mo (190 pm)	−5	0	−2	−7	—

and ref. [11] confirm that the σ phase is rich in Cr and Mo elements. We suggest that the formation of the μ phase is due to the large lattice strain produced by the excess Mo element, which makes the σ phase unable to maintain its tetragonal structure. The release of lattice strain causes the σ phase to transform into the μ phase [11,12].

In Figure 2c and d, it can be seen that a new small block structure is precipitated around the large dendrite. The energy dispersive spectroscopy point analysis and Table 2 reveal that the Mo element content of the dendrites of the as-cast and annealed alloy is higher than that of the interdendrites, and the increase in the Mo content of the main phase may be related to the phase transformation. As the annealing temperature increases, the Mo element content of the dendrites gradually increases from 20.86 to 32.40%, indicating that σ phase is distributed within the dendrites. The release of lattice strain causes the σ phase to transform into the μ phase. Under high temperature annealing treatment, a small amount of μ phase is resolved and re-precipitated into the dendrites. This results in an increased Mo content in the dendrites.

3.3 Thermogravimetric analysis-differential scanning calorimetry (TG-DSC) simultaneous thermal analysis

Figure 3 shows the TG-DSC curve of the FeCoCrNiMo alloy during heating from room temperature to 1,273 K. The TG curve shows that at the beginning of heating up to about 453 K, the alloy powder weight decreases at the highest rate, and then tends to decrease smoothly. The final weight loss is 2.493% during the entire heating process. There are no significant mass changes during the TG test from room temperature to 1,273 K. The result shows that no physical or chemical reactions, such as sublimation and oxidation, occur that alters the quality of the sample [12]. The DSC curve shows a downward trend below 553 K, which is caused by the diffusion of alloying elements into

Table 2: Composition distribution of microscopic area in as-cast and annealed FeCoCrNiMo alloys

State	Position	Nominal chemical composition (at%)				
		Cr	Fe	Co	Ni	Mo
As-cast	DR	22.05	19.12	20.84	17.13	20.86
	ID	25.52	19.10	20.13	16.14	21.11
AT-873 K	DR	22.38	19.76	21.24	16.87	19.75
	ID	25.02	18.81	20.62	15.44	20.11
AT-1,073 K	DR	22.81	20.16	20.75	17.60	18.68
	ID	23.75	17.82	21.88	14.28	22.28
AT-1,273 K	DR	22.35	18.38	22.37	14.10	22.80
	ID	19.28	17.59	23.19	13.79	26.15

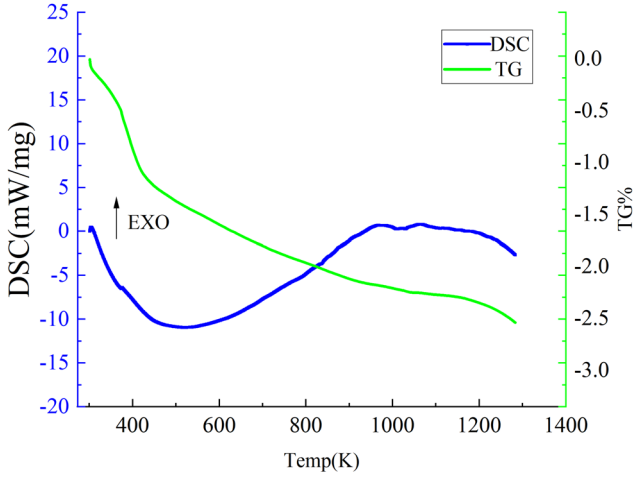

Figure 3: TG-DSC curves of FeCoCrNiMo highentropy alloy.

the FCC solid solution at high temperatures to absorb heat. The rise in the DSC curve in the 553–973 K range may be due to the release of lattice distortion energy from the FCC solid solution. And there is no obvious exothermic or endothermic peak in the whole temperature range, indicating that the FeCoCrNiMo alloy has excellent thermal stability [13].

3.4 Microhardness analysis

Microhardness of the HEAs was measured on the polished cross-sectional surface using a Vickers hardness tester. A load of 200 g and a holding time of 15 s were applied. With the increase in the annealing temperature, the microhardness increases first and then decreases. It can be seen from Table 3 that when the annealing temperature is 1,073 K, the FeCoCrNiMo alloy has the highest microhardness. The average hardness of the alloy is 699.96$HV_{0.2}$, which is about 147$HV_{0.2}$ higher than as-cast. The microhardness of the annealed alloy is higher than that of the as-cast

Table 3: Hardness $HV_{0.2}$ of the FeCoCrNiMo alloy at different annealing temperatures and as-cast

No.	As-cast	AT-873 K	AT-1,073 K	AT-1,273 K
1	565.3	670.5	692.0	617.9
2	544.8	663.6	678.9	605.5
3	542.6	623.9	696.2	615.9
4	534.7	681.1	706.3	647.0
5	575.6	645.3	726.4	649.1
Average	552.60	656.88	699.96	627.08

alloy, and the microstructure of the annealed alloy has a wider area of dendrites.

It can be seen from the XRD pattern that the intensity of the diffraction peaks of the σ phase and μ phase in the alloy is higher at 873 K. The σ phase and μ phase play a role in the strengthening and hardening of the alloy, the hardness of the annealed alloy is higher than the hardness of the cast alloy. At annealing temperature of 1,073 K, the excess Mo element decomposes in the μ phase and the interdendritic structures are re-precipitated to form the σ phase, which makes the alloy hardness reach the maximum. A small amount of the σ phase is redissolved at 1,273 K and the hardness of the alloy is reduced [14]. The annealing process provides sufficient energy for the diffusion of the elements, enhancing inter-element diffusion and displacement. Diffusion and displacement between elements is enhanced and the solid solution strengthening effect is reduced.

3.5 Compression performance analysis

Figure 4 shows the compressive stress–strain curves of FeCoCrNiMo alloy in as-cast and annealed state at different annealed temperatures. The compressive yield strength (σ_y), compressive fracture strength (σ_{max}), and compressive

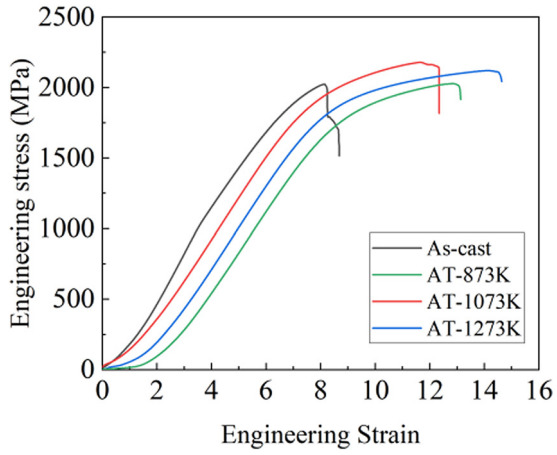

Figure 4: The strain–stress curves of as-cast and annealed FeCoCrNiMo alloys.

Table 4: Room temperature compression performance parameters of as-cast and annealed FeCoCrNiMo alloys

State	σ_y (MPa)	σ_{max} (MPa)	ε_p (%)
As-cast	1308.4	2023.4	8.68
At-873 K	1387.7	2027.3	12.3
At-1,073 K	1530.1	2180.5	12.7
At-1,273 K	1390.9	2030.3	14.1

deformation rate (ε_p) are shown in Table 4. After annealing at 1,073 K, the yield strength and fracture strength of the alloy is 1530.1 and 2180.5 MPa, respectively. After annealing at 1,073 K, the σ phase in the alloy increases. The precipitation strengthening effect is significant, so the yield strength increases [15,16]. With the increase in the annealing temperature, the microstructure of alloy is gradually refined and the strain capacity is enhanced. After annealing at 1,273 K, the highest compressive deformation rate is 14.1%, which is 5.4% higher than that of as-cast alloy.

3.6 Fracture morphology

Figure 5 shows the fracture morphologies of the FeCoCrNiMo alloy. The fracture mechanism is intergranular brittle fracture and cleavage fracture [17]. This result is in accordance with the compression results shown in Figure 4. When cleavage fracture occurs, the crack growth rate in different areas of the cleavage surface is not consistent, which will cause a small amount of tearing cracks [18–21].

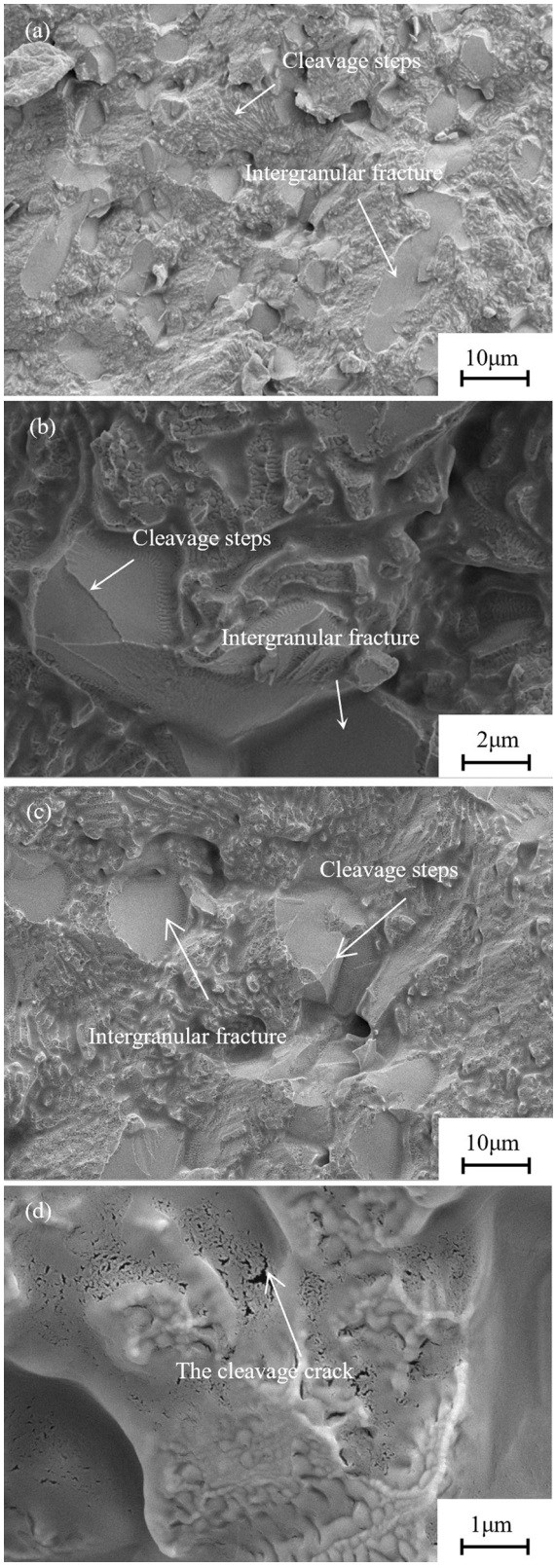

Figure 5: SEM images of the compression fracture of FeCoCrNiMo alloy: (a) As-cast, (b) AT-873 K, (c) AT-1,073 K, and (d) AT-1,273 K.

In addition, XRD analysis shows the presence of σ phase in the alloy. The relevant literature [22,23] shows that the presence of the σ phase in the alloy causes a significant reduction in the ductility of the alloy, which can occur even if only a small amount of the σ phase precipitates.

The above results indicate that the FeCoCrNiMo alloy exhibits brittle fracture. This can be attributed to the lattice distortion and the presence of brittle intermetallic compounds [24–26], which are inherently very brittle similar to the other types of intermetallic compounds [27–30]. Due to the poor ductility of brittle intermetallic compounds in FeCoCrNiMo alloy, the alloy shows a strong tendency to form microcavities in crack propagation.

4 Conclusion

1. The microstructure of the as-cast FeCoCrNiMo alloy was composed of FCC phase, σ phase, and μ phase. The μ phase disappeared after annealing at 1,073 K and the σ phase was formed to re-precipitate in the dendrites.
2. The hardness at different annealing temperatures was higher than that of as-cast alloys. The analysis results showed that the precipitation of μ phase and σ phase increased the hardness of the alloy. After annealing at 1,073 K, the alloy hardness was 699.96$HV_{0.2}$ with the highest average hardness. There was no more obvious peak in the DSC curve, indicating excellent thermal stability of FeCoCrNiMo alloy.
3. FeCoCrNiMo alloy showed the best compressive mechanical properties after annealing at 1,073 K. The compressive strength of this alloy was 2180.5 MPa, and the yield strength is 1530.1 MPa. Fracture analysis showed that the compression fracture mechanism of FeCoCrNiMo alloy in the annealed state was intergranular brittle fracture and cleavage fracture.

Acknowledgments: This work has been supported by the Natural Science Foundation of the Higher Education Institutions of Anhui Province under Grant No. KJ2020ZD42.

Funding information: Natural Science Foundation of the Higher Education Institutions of Anhui Province, China (KJ2020ZD42).

Author contributions: Lei Sheng: resources, writing – original draft, writing – review & editing, methodology, and formal Analysis; Xue Zhengwei: writing – original draft, writing – review & editing, methodology, and formal Analysis; Liu Yafeng: writing – original draft, writing – review & editing, methodology, and formal Analysis; Li Yun: project administration, management and coordination responsibility for the research activity planning and execution; Jiang Dongsheng: project administration, management and coordination responsibility for the research activity planning and execution; Wang Ping: project administration, management and coordination responsibility for the research activity planning and execution.

Conflict of interest: The authors declared that they have no conflicts of interest in this work and do not have any commercial or associative interest that represents a conflict of interest in connection with the work submitted.

Data availability statement: The datasets generated during and/or analyzed during the current study are available from the corresponding author on reasonable request.

References

[1] Li, Y., P. K. Liaw, and Y. Zhang. Microstructures and properties of the low-density $Al_{15}Zr_{40}Ti_{28}Nb_{12}M(Cr,Mo,Si)_5$ high-entropy alloys. *Metals*, Vol. 12, 2022, id. 496.

[2] Chen, J., X. Zhou, W. Wang, B. Liu, Y. Lv, W. Yang, et al. A review on fundamental of high entropy alloys with promising high-temperature properties. *Journal of Alloys and Compounds*, Vol. 760, 2018, pp. 15–30.

[3] Çam, G. and M. Koçak. Progress in joining of advanced materials. *International Metals Reviews*, Vol. 43, No. 1, 1998, pp. 1–44.

[4] Çam, G. and M. Koçak. Progress in joining of advanced materials - part II: Joining of metal matrix composites and joining of other advanced materials. *Science and Technology of Welding & Joining*, Vol. 3, No. 4, 1998, pp. 159–175.

[5] Çam, G., A. Fischer, R. Ratjen, J. F. dos Santos, and M. Koçak. Properties of laser beam welded superalloys inconel 625 and 718. *Proceedings of 7th European Conference on Laser Treatment of Materials (ECLAT '98), September 21–23, 1998, Hannover, Germany*, B. L. Mordike, pub, ed., Werkstoff-Informationsgeselschaft mbH, Frankfurt, 1998, pp. 333–338.

[6] Vallimanalan, A., S. P. Kumaresh Babu, S. Muthukumaran, M. Murali, V. Gaurav, and R. Mahendran. Corrosion behaviour of thermally sprayed Mo added AlCoCrNi high entropy alloy coating. *Materials Today: Proceedings*, Vol. 27, No. Part 3, 2020, pp. 2398–2400.

[7] Dai, C., T. Zhao, C. Du, Z. Liu, and D. Zhang. Effect of molybdenum content on the microstructure and corrosion behavior of FeCoCrNiMox high-entropy alloys. *Journal of Materials Science & Technology*, Vol. 46, 2020, pp. 64–73.

[8] Shun, T.-T., L.-Y. Chang, and M.-H. Shiu. Microstructure and mechanical properties of multiprincipal component CoCrFeNiMox alloys. *Materials Characterization*, Vol. 70, 2012, pp. 63–67.

[9] Liu, W. H., Z. P. Lu, J. Y. He, J. H. Luan, Z. J. Wang, B. Liu, et al. Ductile $CoCrFeNiMo_x$ high entropy alloys strengthened by hard intermetallic phases. *Acta Mater*, Vol. 116, 2016, pp. 332–342.

[10] Liu, W. H., Z. P. Lu, J. Y. He, J. H. Luan, Z. J. Wang, B. Liu, et al. Ductile CoCrFeNiMo$_x$ high entropy alloys strengthened by hard intermetallic phases. *Acta Materialia*, Vol. 116, 2016, pp. 332–342.
[11] Niu, Z., Y. Wang, C. Geng, J. Xu, and Y. Wang. Microstructural evolution, mechanical and corrosion behaviors of as-annealed CoCrFeNiMo$_x$ (x = 0, 0.2, 0.5, 0.8, 1) high entropy alloys. *Journal of Alloys and Compounds*, Vol. 820, 2020, id. 153273.
[12] Fan, A.-C., J.-H. Li, and M.-H. Tsai. On the phase constituents of three CoCrFeNiX (X = Cr, Mo, W) high-entropy alloys after prolonged annealing. *Materials Chemistry and Physics*, Vol. 276, 2022, id. 125431.
[13] Li, W. P., X. G. Wang, B. Liu, Q. H. Fang, and C. Jiang. Fracture mechanisms of a Mo alloyed CoCrFeNi high entropy alloy: *in-situ* SEM investigation. *Materials Science and Engineering: A*, Vol. 723, 2018, pp. 79–88.
[14] Liu, Y., Y. Xie, S. Cui, Y. Yi, X. Xing, X. Wang, et al. Effect of Mo element on the mechanical properties and tribological responses of CoCrFeNiMo$_x$ high-entropy alloys. *Metals*, Vol. 11, 2021, id. 486.
[15] Sui, Q., Z. Wang, J. Wang, S. Xu, B. Liu, Q., et al. Additive manufacturing of CoCrFeNiMo eutectic high entropy alloy: microstructure and mechanical properties. *Journal of Alloys and Compounds*, Vol. 913, 2022, id. 165239.
[16] Cao, B. X., T. Yang, L. Fan, J. H. Luan, Z. B. Jiao, and C. T. Liu. Refractory alloying additions on the thermal stability and mechanical properties of high-entropy alloys. *Materials Science and Engineering A*, Vol. 797, 2020, id. 140020.
[17] Li, N., W. Chen, J. He, J. Gu, Z. Wang, Y., et al. Dynamic deformation behavior and microstructure evolution of CoCrNiMo$_x$ medium entropy alloys. *Materials Science and Engineering: A*, Vol. 827, 2021, id. 142048.
[18] Li, W. P., X. G. Wang, B. Liu, Q. H. Fang, and C. Jiang. Fracture mechanisms of a Mo alloyed CoCrFeNi high entropy alloy: *in-situ* SEM investigation. *Materials Science and Engineering: A*, Vol. 723, 2018, pp. 79–88.
[19] Chung, D. H., X. D. Liu, and Y. Yang. Fracture of sigma phase containing Co–Cr–Ni–Mo medium entropy alloys. *Journal of Alloys and Compounds*, Vol. 846, 2020, id. 156189.
[20] Wang, J., J. Zou, H. Yang, Z. Liu, and S. Ji. High strength and ductility of an additively manufactured CrCoNi medium-entropy alloy achieved by minor Mo doping. *Materials Science and Engineering: A*, Vol. 843, 2022, id. 143129.
[21] Jiao, W., H. Jiang, D. Qiao, J. He, H. Zhao, Y. Lu, et al. Effects of Mo on microstructure and mechanical properties of Fe2Ni2CrMo$_x$ eutectic high entropy alloys. *Materials Chemistry and Physics*, Vol. 260, 2021, id. 124175.
[22] Chuang, M.-H., M.-H. Tsai, C.-W. Tsai, N.-H. Yang, S.-Y. Chang, J.-W. Yeh, et al. Intrinsic surface hardening and precipitation kinetics of $Al_{0.3}CrFe_{1.5}MnNi_{0.5}$ multi-component alloy. *Journal of Alloys and Compounds*, Vol. 551, 2013, pp. 12–18.
[23] Hall, E. O. and S. H. Algie The sigma phase. *Metallurgical Research*, Vol. 11, 1966, pp. 61–88.
[24] Qin, G., R. Chen, H. Zheng, H. Fang, L. Wang, Y. Su, et al. Strengthening FCC-CoCrFeMnNi high entropy alloys by Mo addition. *Journal of Materials Science & Technology*, Vol. 35, No. 4, 2019, pp. 578–583.
[25] Man, J., B. Wu, G. Duan, L. Zhang, G. Wan, L., et al. The synergistic addition of Al, Ti, Mo and W to strengthen the equimolar CoCrFeNi high-entropy alloy via thermal-mechanical processing. *Journal of Alloys and Compounds*, Vol. 902, 2022, id. 163774.
[26] Moon, J., E. Tabachnikova, S. Shumilin, T. Hryhorova, Y. Estrin, J., et al. Deformation behavior of a Co-Cr-Fe-Ni-Mo medium-entropy alloy at extremely low temperatures. *Materials Today*, Vol. 50, 2021, pp. 55–68.
[27] Cam, G., H. M. Flower, and D. R. F. West. Constitution of Ti-Al-C alloys in the temperature range 1,250-750°C. *Materials Science and Technology*, Vol. 7, No. 6, 1991, pp. 505–511.
[28] Çam, G., H. Clemens, R. Gerling, and M. Koçak. Diffusion bonding of fine grained gamma-TiAl sheets. *Zeitschrift fuer Metallkunde*, Vol. 90, No. 4, 1999, pp. 284–288.
[29] Çam, G., G. İpekoğlu, K.-H. Bohm, and M. Koçak. Investigation into the microstructure and mechanical properties of diffusion bonded TiAl alloys. *Journal of Materials Science*, Vol. 41, No. 16, 2006, pp. 5273–5282.
[30] Çam, G., K.-H. Bohm, J. Müllauer, and M. Koçak. The fracture behavior of diffusion-bonded duplex gamma TiAl. *JOM*, Vol. 48, No. 11, 1996, pp. 66–68.